ARTICLE

Check for updates

Tropical extreme droughts drive long-term increase in atmospheric CO_2 growth rate variability

Xiangzhong Luo [1,2,3 ✉] & Trevor F. Keenan [1,2 ✉]

The terrestrial carbon sink slows the accumulation of carbon dioxide (CO_2) in the atmosphere by absorbing roughly 30% of anthropogenic CO_2 emissions, but varies greatly from year to year. The resulting variations in the atmospheric CO_2 growth rate (CGR) have been related to tropical temperature and water availability. The apparent sensitivity of CGR to tropical temperature (γ_{CGR}^T) has changed markedly over the past six decades, however, the drivers of the observation to date remains unidentified. Here, we use atmospheric observations, multiple global vegetation models and machine learning products to analyze the cause of the sensitivity change. We found that a threefold increase in γ_{CGR}^T emerged due to the long-term changes in the magnitude of CGR variability (i.e., indicated by one standard deviation of CGR; STD_{CGR}), which increased 34.7% from 1960-1979 to 1985-2004 and subsequently decreased 14.4% in 1997-2016. We found a close relationship ($r^2 = 0.75$, $p < 0.01$) between STD_{CGR} and the tropical vegetated area (23°S – 23°N) affected by extreme droughts, which influenced 6-9% of the tropical vegetated surface. A 1% increase in the tropical area affected by extreme droughts led to about 0.14 Pg C yr^{-1} increase in STD_{CGR}. The historical changes in STD_{CGR} were dominated by extreme drought-affected areas in tropical Africa and Asia, and semi-arid ecosystems. The outsized influence of extreme droughts over a small fraction of vegetated surface amplified the interannual variability in CGR and explained the observed long-term dynamics of γ_{CGR}^T.

[1] Climate and Ecosystem Sciences Division, Lawrence Berkeley National Laboratory, Berkeley, CA, USA. [2] Department of Environmental Science, Policy and Management, UC Berkeley, Berkeley, CA, USA. [3] Department of Geography, National University of Singapore, Singapore, Singapore.
✉email: xzluo.remi@nus.edu.sg; trevorkeenan@berkeley.edu

Year-to-year variations in the CGR (ΔCGR; detrended CGR) mainly reflect changes in the terrestrial carbon sink[1], with a relatively small contribution from changes in ocean uptake and land use emissions[2–4 but see 5]. ΔCGR is highly variable, ranging between −2.0 and 2.5 PgC yr^{-1} [6], and the majority of that variability is driven by changes in tropical climate[6–10] through the influence of climate on the tropical terrestrial ecosystems[2,11,12], among which tropical forests[1] or semi-arid ecosystems[13,14] (i.e., mostly the semi-arid ecosystems in the tropics[15]) or both[15] have been reported to play the primary role. In particular, ΔCGR is sensitive to changes in temperature and water storage over the tropical land surface[1,6,8,9,16]. Positive anomalies of mean annual temperature over tropical land (ΔMAT) have been associated with a higher CGR, potentially due to the suppression of tropical photosynthesis[17,18] and/or enhanced respiration[17,19,20], as have drier years[9,16]. Notably, the apparent temperature sensitivity of CGR (γ_{CGR}^{T}, see Methods) has been found to exhibit long-term dynamics, and has doubled between 1960 and the past decade[8,10]. In contrast to γ_{CGR}^{T}, the dynamics of the apparent sensitivity of CGR to water (γ_{CGR}^{W}) are less well understood, with conflicting reports suggesting either a non-evident global water sensitivity at the global scale[6,21] or a strong coupling between ΔCGR and satellite-derived terrestrial water storage[9] and lagged precipitation[16]. Recent evidence demonstrated that γ_{CGR}^{T} and γ_{CGR}^{W} are related due to the land-atmosphere coupling by soil moisture[22], suggesting a potential change in γ_{CGR}^{W} over time.

The underlying mechanisms for long-term changes in the climate sensitivity of CGR (i.e., γ_{CGR}^{T} and γ_{CGR}^{W}) remain elusive, as process-based models demonstrate different climate sensitivities from observations[8,9]. Empirical evidence suggests that γ_{CGR}^{T} is higher in years with greater tropical aridity[8], implying a role of tropical water availability in modulating γ_{CGR}^{T}. Water availability is known to influence land-atmosphere CO_2 exchange at seasonal and annual timescales through stomatal responses to atmospheric water stress or the downregulation of plant metabolism due to soil moisture deficits[23,24]. Extreme water deficits can further induce changes in land-atmosphere CO_2 exchange over longer time scales, through lagged responses and legacy effects of terrestrial ecosystems (i.e. mortality[25–27], fire[28], recovery[29,30] and deadwood decomposition[31]). This hierarchy of water-related processes can modulate CGR and manifest as the changes in γ_{CGR}^{T}, especially under extreme drought conditions. In fact, recent evidence has suggested that extreme droughts over small areas in Amazon and Australia have a disproportionally large contribution to the global carbon cycle[32,33], highlighting a potential role of tropical extreme droughts in modulating γ_{CGR}^{T}.

Therefore, we hypothesize that the long-term changes in γ_{CGR}^{T} and γ_{CGR}^{W} over the past six decades are related to changes in extreme droughts over tropical vegetated lands (23°S–23°N) and our objective is to test the hypothesis. However, estimates of apparent climate sensitivities vary between methods and climate data used[6,8,9] (Supplementary Fig. 1), and this uncertainty hinders attribution. We thus focus our examination on long-term CGR variability (i.e., indicated by one standard deviation of CGR within a time frame of decades; STD$_{CGR}$), which underlies the dynamics of derived climate sensitivities (see Methods). Specifically, we examined the long-term changes in γ_{CGR}^{T} and γ_{CGR}^{W} estimated from multiple mainstream methods[8,9], and related the best estimates of γ_{CGR}^{T} and γ_{CGR}^{W} to STD$_{CGR}$. We further examined the relationship between STD$_{CGR}$ and tropical droughts, using several key indicators of tropical water availability, an ensemble of dynamic global vegetation models[34], and the FLUXCOM machine learning products[21] based on observations from the global FLUXNET network (see Methods).

Results

Long-term changes in CGR and its climate sensitivities. We used nine competing methods to derive γ_{CGR}^{T} and γ_{CGR}^{W} from ΔCGR for every 20-year moving window between 1959 and 2016 (Table 1; Supplementary Fig. 1; see Methods). Predictors considered include anomalies of tropical mean annual temperature (ΔMAT), mean annual precipitation (ΔMAP), mean shortwave radiation(ΔRAD), 4-month lagged precipitation (ΔMAP$_{lag}$), reconstructed satellite-derived terrestrial water storage (ΔTWS) and interactions of temperature and water proxies, in univariate or multivariate linear regression models (Table 1; Supplementary Fig. 1; see Methods). Following model selection based on minimizing predictor collinearity, which can cause artificial temporal changes in the derived coefficients, we quantified γ_{CGR}^{T} and γ_{CGR}^{W} based on a multivariate linear regression of ΔCGR on ΔMAT, ΔMAP and ΔRAD (model M1, Table 1, see methods). γ_{CGR}^{T} was significant ($p < 0.05$) in every 20-year window (Fig. 1a), increasing threefold between 1960 and 1999 (1960−1979: 1.83 ± 0.45 PgC yr^{-1} K^{-1} (mean ± s.d.); 1980−1999: 5.49 ± 0.53 PgC yr^{-1} K^{-1}), consistent with previous reports[8,10], and decreasing by 33.6% in the most recent two decades (1997−2016: 3.64 ± 0.53 PgC yr^{-1} K^{-1}) (Fig. 1a). In contrast, γ_{CGR}^{W} was not significant ($p > 0.05$) in most 20-year windows and the sensitivity of CGR to tropical TWS (γ_{CGR}^{TWS}) derived from competing models (M3, M5, M8) was also not significant (Fig. 1; Supplementary Fig. 1).

We examined the ability of 15 Dynamic Global Vegetation Models (DGVMs)[35] and 3 machine learning products from the FLUXCOM project[21] to characterize long-term changes in the

Table 1 The performance of nine competing models (M1-M9) to derive the temperature sensitivity (γ_{CGR}^{T}) and the water sensitivity of CGR (γ_{CGR}^{W}).

Models	Time range	Adj. R^2	AIC	VIF	Reference
M1: $\triangle CGR = \gamma_{CGR}^{T}\triangle MAT + \gamma_{CGR}^{W}\triangle MAP + \gamma_{CGR}^{R}\triangle RAD$	1959–2016	0.47 ± 0.09	46.9 ± 3.6	1.25 ± 0.08	8
M2: $\triangle CGR = \gamma_{CGR}^{T}\triangle MAT + \gamma_{CGR}^{W}\triangle MAP + \gamma_{CGR}^{R}\triangle RAD + \gamma_{CGR}^{i}(\triangle MAT \times \triangle MAP)$	1959–2016	0.46 ± 0.10	47.8 ± 2.9	1.46 ± 0.16	
M3: $\triangle CGR = \gamma_{CGR}^{T}\triangle MAT + \gamma_{CGR}^{W}\triangle TWS + \gamma_{CGR}^{R}\triangle RAD$	1980–2016	0.56 ± 0.04	44.6 ± 2.5	1.50 ± 0.22	9
M4: $\triangle CGR = \gamma_{CGR}^{T}\triangle MAT + \gamma_{CGR}^{W}\triangle MAP_{lag} + \gamma_{CGR}^{R}\triangle RAD$	1960–2016	0.50 ± 0.16	45.0 ± 5.8	2.49 ± 0.46	9
M5: $\triangle CGR = \gamma_{CGR}^{T}\triangle MAT + \gamma_{CGR}^{W}\triangle TWS + \gamma_{CGR}^{R}\triangle RAD + \gamma_{CGR}^{i}(\triangle MAT \times \triangle TWS)$	1980–2016	0.59 ± 0.04	44.0 ± 3.0	1.57 ± 0.29	
M6: $\triangle CGR = \gamma_{CGR}^{T}\triangle MAT + \gamma_{CGR}^{W}\triangle MAP_{lag} + \gamma_{CGR}^{R}\triangle RAD + \gamma_{CGR}^{i}(\triangle MAT \times \triangle MAP_{lag})$	1960–2016	0.50 ± 0.18	45.4 ± 7.0	2.64 ± 0.43	
M7: $\triangle CGR = \gamma_{CGR}^{T}\triangle MAT$	1959–2016	0.46 ± 0.13	45.6 ± 3.1	–	8, 10
M8: $\triangle CGR = \gamma_{CGR}^{W}\triangle TWS$	1959–2016	0.31 ± 0.06	51.6 ± 2.2	–	9
M9: $\triangle CGR = \gamma_{CGR}^{W}\triangle MAP_{lag}$	1980–2016	0.42 ± 0.17	46.4 ± 5.4	–	16

Akaike information criterion (AIC) indicate the parsimony of model and variance inflation factor (VIF) indicate the collinearity of predictors. The model performance is evaluated for every 20-year window, therefore the statistical indicators (i.e., R^2, AIC, and VIF) are the mean of models from every window and uncertainty is one standard deviation. The interaction terms were normalized before used in the regression models.
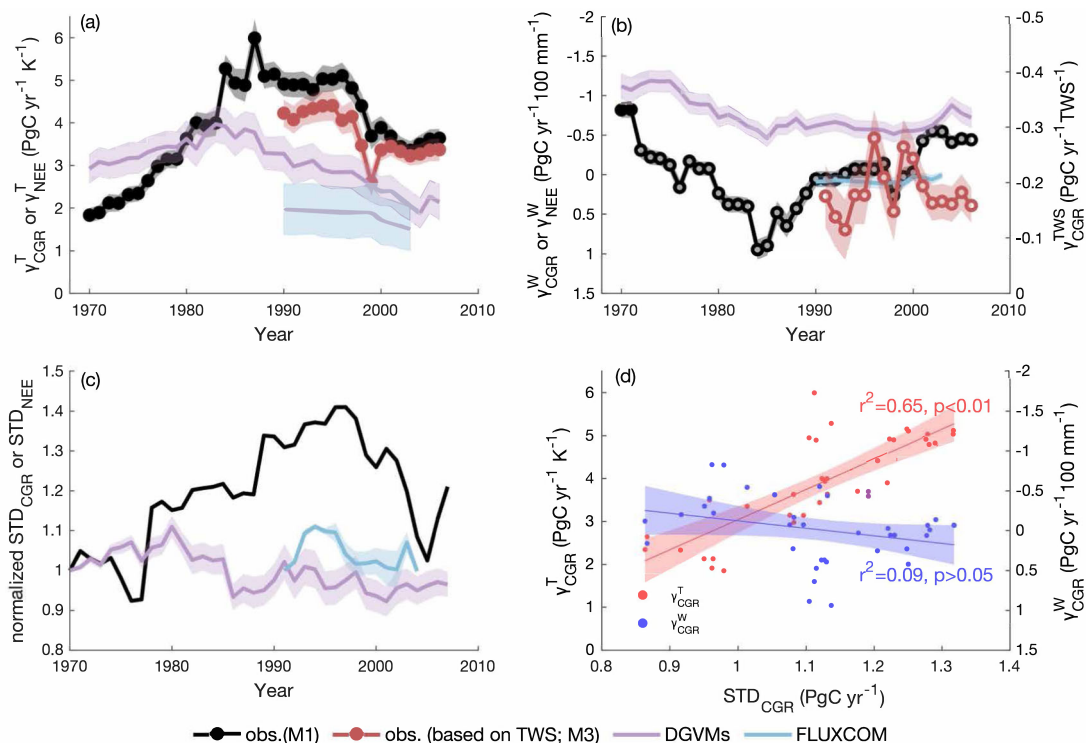
Fig. 1 Temporal dynamics of the climate sensitivities of the atmospheric CO_2 growth rate (CGR) and net ecosystem exchange (NEE). a Temporal dynamics of the apparent temperature sensitivity of observed CGR (γ_{CGR}^T) or modeled NEE (γ_{NEE}^T); **b** temporal dynamics of the apparent water sensitivity of CGR (γ_{CGR}^W) or modeled NEE (γ_{NEE}^W). The observed climate sensitivities are calculated using multivariate regressions of ΔCGR to ΔMAT and either ΔMAP or ΔTWS for each 20-year window from 1959 to 2016 (see Methods, model M1 and M3). A solid circle marker indicates significant ($p < 0.05$) sensitivities of CGR to climate variables in that 20-year window, while open circles indicate insignificant ($p > 0.05$) sensitivities. Black and red shaded areas indicate one standard error of climate sensitivities derived from 100 bootstrap estimates, considering the CGR uncertainty of 0.2 PgC yr^{-1} [61]. Other shaded areas indicate the intermodel variations of climate sensitivity (i.e., one standard error). **c** The long-term dynamics of the variance of CGR (STD_{CGR}) and NEE (STD_{NEE}). STD_{CGR} and STD_{NEE} were calculated for every 20-year window from 1959 to 2016, and normalized by their respective first value (i.e., the STD_{CGR} and STD_{NEE} of 1959 to 1978). **d** The relationships between climate sensitivities of CGR (i.e., γ_{CGR}^T and γ_{CGR}^W) and STD_{CGR} (shading: 95% confidence interval). CGR in the years 1991–1993 are affected by the eruption of Mt Pinatubo and thus excluded.

CGR climate sensitivity. We found that both DGVMs and the machine learning products mischaracterized the temperature sensitivity (γ_{NEE}^T) of terrestrial net ecosystem exchange (NEE), the primary driver for the variation in CGR (Fig. 1a, b). γ_{NEE}^T from DGVMs increased from 3.20 ± 0.35 PgC yr^{-1} K^{-1} in the 1970s to 3.65 ± 0.42 PgC yr^{-1} K^{-1} in the 1980s, and decreased to 2.19 ± 0.37 PgC yr^{-1} K^{-1} in the 2000s, however, the magnitude of change was much smaller than that of observed γ_{CGR}^T. Meanwhile, γ_{NEE}^T from FLUXCOM was relatively constant, around 1.84 ± 0.58 PgC yr^{-1} K^{-1}. Models such as those tested here are frequently used to infer the influence of soil moisture on global carbon cycle dynamics[13,14,21,23]. The discrepancy between observed γ_{CGR}^T and modeled γ_{NEE}^T we identified implies limitations in process-based models and machine learning methods, and calls into question their utility for diagnosing long-term changes in climate sensitivities.

Considering the DGVMs and FLUXCOM products we examined were forced by a similar climate dataset (i.e., CRU and CRU-NCEP, see Methods) that we used to obtain γ_{CGR}^T and γ_{CGR}^W, the disagreement between the observed and modeled climate sensitivities can only be attributed to the difference between the observed variance of CGR (i.e. indicated by one standard deviation of CGR over the 20-year window; STD_{CGR}) and the modeled variance of NEE (i.e. indicated by one standard deviation of annual NEE over the 20-year window; STD_{NEE}). Indeed, we found that the STD_{CGR} increased 34.7% from

0.98 PgC yr^{-1} in 1960-1979 to 1.32 PgC yr^{-1} in 1985–2004, and then decreased slightly by 14.4% to 1.13 PgC yr^{-1} in 1997–2016 (Fig. 1c), and such a change in STD_{CGR} underlies the dynamics of γ_{CGR}^T we detected ($r^2 = 0.65$; Fig. 1d). The strong dependence of γ_{CGR}^T on STD_{CGR} was not affected by autocorrelations in the time series (Supplementary Fig. 3a, c). In contrast, STD_{NEE} from DGVMs and FLUXCOM demonstrated no clear variation, with STD_{NEE} fluctuating by only -8 to 10% over time (Fig. 1c).

Tropical extreme droughts associated with changes in STD_{CGR}. The long-term dynamics in STD_{CGR} over the past 60 years were neither explained by the changes in the variability of ocean carbon uptake, emissions due to land use and land cover change[5,20] and emissions from fires[36] (Supplementary Fig. 2), nor by the estimates of NEE from DGVMs. Motivated by a previous study reporting the dependence of γ_{CGR}^T on multiyear average aridity indexes for tropics[8], we examined the influence of long-term tropical water availability on STD_{CGR}. Our result showed that 20-year average tropical TWS, soil water content and mean annual precipitation ($\overline{TWS}$, $\overline{SWC}$, $\overline{MAP}$) were negatively and significantly related to the changes in STD_{CGR} ($r^2 = 0.68$, 0.68, 0.65 ± 0.09, respectively; $p < 0.01$; Fig. 2a), showing that CGR was more variable in drier decades. In comparison, 20-year average MAT ($\overline{MAT}$) and vapor pressure deficit ($\overline{VPD}$) explained much less variance in STD_{CGR} ($r^2 = 0.30 \pm 0.02$, 0.21, respectively;
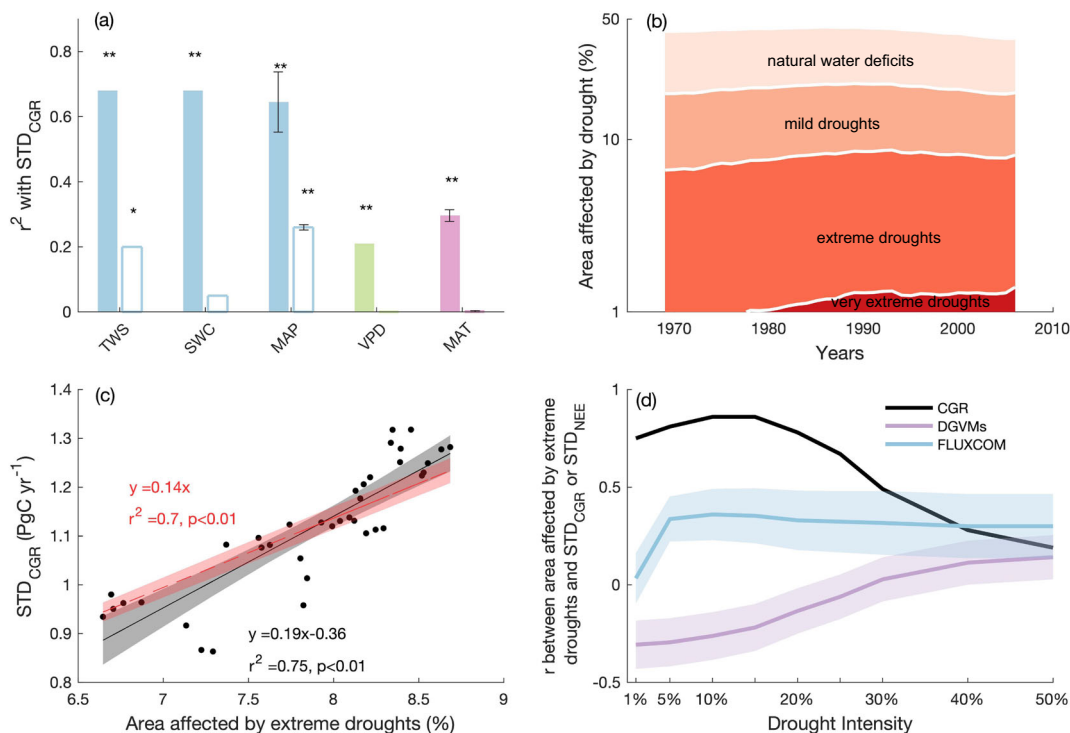
Fig. 2 The relationships between the changes in STD$_{CGR}$ and tropical water availability and drought-affected area. a The variance in STD$_{CGR}$ explained by long-term water availability or temperature in the tropics, as represented by 20-year average terrestrial water storage ($\overline{TWS}$), soil water content ($\overline{SWC}$), mean annual precipitation ($\overline{MAP}$), vapor pressure deficit ($\overline{VPD}$) and mean annual temperature ($\overline{MAT}$). The error bars indicate the uncertainty (one standard error) in r^2 when using alternative precipitation and temperature datasets (see Methods); the hollow bars indicate the variance in STD$_{CGR}$ explained by long-term tropical water availability or temperature, after accounting for autocorrelations in variables using the Cochrane-Ocrutt procedure (see Methods). *$p < 0.1$, **$p < 0.01$; note the correlations between STD$_{CGR}$ and $\overline{TWS}$, $\overline{SWC}$ and $\overline{MAP}$ are negative while the correlation between STD$_{CGR}$ and $\overline{VPD}$ and $\overline{MAT}$ are positive; **b** the temporal dynamics of the percentage of tropical vegetated area affected by droughts of different intensities; drought intensity is defined by the percentile of local monthly precipitation across the whole study period (1959–2016), where the bottom 1% precipitation indicates very extreme droughts, bottom 1–10% precipitation indicates extreme droughts, 10–25% precipitation indicates mild droughts, and 25–50% precipitation indicates natural water deficits; the y-axis is log-transformed; **c** The relationship between STD$_{CGR}$ and the tropical vegetated area affected by extreme and very extreme droughts. The shadings indicate the 95% confidence intervals of the linear regressions. The linear regressions with and without a y intercept were examined; **d** the correlation coefficient (r) between observed STD$_{CGR}$ or modeled (i.e., DGVMs and FLUXCOM) STD$_{NEE}$ and areas affected by droughts of different intensities in the tropics. Drought intensities are defined by the bottom percentiles (e.g., 1%, 10%, 25%) of monthly precipitation. Shaded areas indicate the intermodel variation of r (i.e., one standard error).

$p < 0.01$). We then removed the autocorrelations of the aforementioned 20-year average time series and found only the significant influence of $\overline{TWS}$ ($p < 0.1$) and $\overline{MAP}$ ($p < 0.01$) on STD$_{CGR}$ persisted (Fig. 2a; see Methods), highlighting a role of tropical water availability in modulating STD$_{CGR}$. Note that the removal of autocorrelation resulted in a smaller deterministic coefficient (r^2) between long-term water availability and STD$_{CGR}$, which is expected given the correction removes all the short-term variation in time series. As $\overline{MAP}$ showed the strongest explanatory power after considering autocorrelations in these explanatory time series, we used precipitation as the primary indicator for further analysis.

The observed negative couplings between tropical $\overline{TWS}$ and $\overline{MAP}$ and STD$_{CGR}$ (Fig. 2a) imply a considerable influence of tropical drought on long-term land-atmosphere CO_2 exchange. Following the definition of meteorological drought[37,38], we analysed drought occurrence in tropical regions over the past 60 years. We used percentiles of local monthly precipitation to classify different degrees of drought—from very extreme droughts (i.e., bottom 1% of precipitation), to extreme droughts (i.e., bottom 1–10%), to mild droughts (i.e., bottom 10–25%) and up to

natural water deficits (i.e., bottom 25–50%). We quantified the drought-affected area for each month, and calculated standardized annual drought-affected area using drought durations (see Methods). From 1959 to 2016, the tropical vegetated area affected by very extreme droughts increased from 0 to 1.4%, and the area affected by extreme droughts increased from 5.8% to 7.3% then slightly decreased to 6.7% (Fig. 2b). In contrast, the tropical area influenced by mild droughts decreased from 11.8% to 10.5% and the area influenced by natural water deficits decreased from 24.0% to 19.1% (Fig. 2b).

We examined the relationship between STD$_{CGR}$ and areas affected by different categories of drought, and found the changes in the extreme drought-affected area explained 75% of the variance in STD$_{CGR}$ ($p < 0.01$; Fig. 2c, d). Since the extreme droughts influenced around 6% to 9% of the tropical vegetated land surface, our result indicates a substantially outsized influence of extreme droughts on STD$_{CGR}$. To assess the robustness of the results, we removed the temporal autocorrelation in time series using two alternative methods and found that our conclusions are not qualitatively impacted by autocorrelation (Supplementary Fig. 3; see Methods). We found a 1% increase in
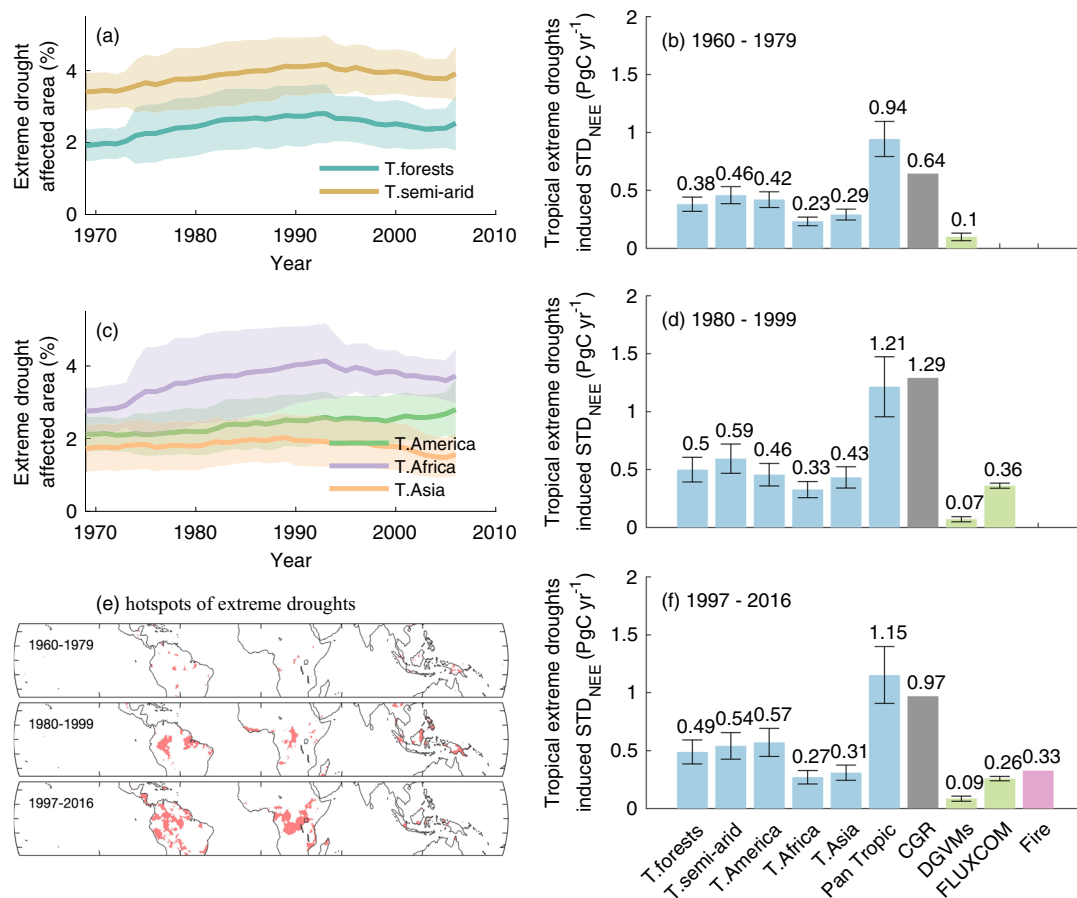
Fig. 3 Spatial distribution of tropical extreme droughts and drought-induced changes in STD$_{CGR}$ over the past 60 years. a the fraction of tropical vegetated area affected by extreme droughts for tropical (T.) forests and semi-arid regions. The solid line presents the mean fraction of tropical vegetated area affected by extreme droughts in every 20 years window from 1959 to 2016, with the x axis indicating the center of each window. The shaded area indicates the variability of the fraction (e.g., one standard deviation) in each 20-year window; **c** the fraction of tropical vegetated area affected by extreme droughts for tropical America, tropical Africa, and tropical Asia; **e** the changes of the extreme drought hotspots in three 20 years periods. Hotspots are defined as regions that are under extreme droughts for more than 10% of time; **b, d, f** The impacts of tropical extreme droughts on global net ecosystem exchange variability (STD$_{NEE}$) in three independent 20-year periods. The extreme drought-induced STD$_{NEE}$ was estimated using the relationship between drought-affected area and STD$_{CGR}$ (shown in Fig. 2c) in combination with a spatial weight based on FLUXCOM NEE (see Methods). The average impact from each region is indicated by the numbers in the figure, while the error bars indicate the variability of extreme drought-induced STD$_{NEE}$ in each 20-year window propagated from the variability in the fraction of area affected by extreme droughts shown in (**a**) and (**c**). The impact of droughts estimated by DGVMs and FLUXCOM are included as reference, where the error bars indicate the intermodel variations. Fire emissions are obtained from Global Fire Emissions Database (GFED4s).

extreme drought-affected area corresponded to a 0.14 Pg C yr^{-1} increase in STD$_{CGR}$. In contrast, mild droughts had a limited influence on STD$_{CGR}$, as the addition of mild droughts reduced the coupling between drought-affected area and STD$_{CGR}$ (Fig. 2d). We repeated the analysis using STD$_{NEE}$ from DGVMs, and found models was unable to characterize the outsized influence of extreme droughts, with negative correlations between extreme drought-affected area and STD$_{NEE}$ across all drought categories (Fig. 2d; Supplementary Fig. 5b). In comparison, STD$_{NEE}$ estimated by FLUXCOM was positively but weakly related to the area affected by extreme droughts, implying that the data-driven NEE product was able to capture the influence of extreme droughts effect better than DGVMs, though with substantial underestimation of the effect (Fig. 2d; Supplementary Fig. 5c).

Spatial variation in extreme drought-induced changes in STD$_{CGR}$. Extreme droughts happened unevenly over time and space, and thus contributed differently to the variation of STD$_{CGR}$.

Among the three continents, tropical Africa had more area affected by extreme droughts (c. 3.62 ± 0.91% of tropical vegetated land surface) in the past 60 years than tropical America (c. 2.39 ± 0.63%) and tropical Asia (c. 1.82 ± 0.65%). The extreme drought-affected area in the tropical America showed a positive trend over time, while areas affected by droughts in tropical Africa and tropical Asia increased before the 1990s and then plateaued or decreased in the recent two decades (Fig. 3c), contributing to the recent decrease in STD$_{CGR}$. The areas most threatened by extreme droughts were located in tropical America and Africa, however, the location of drought hotspots demonstrated also long-term variations, as drought-affected areas were more concentrated in the 1980s and the 1990s than the recent two decades (Fig. 3e). In parallel, extreme droughts influenced more semi-arid ecosystems (c. 3.85 ± 0.72% of vegetated land surface) than forests (c. 2.47 ± 0.71%), and the drought-affected area of both ecosystems increased from the 1960s to the 1990s and decreased in the 2000s (Fig. 3a).

To further quantify the regional contributions of extreme droughts to STD$_{CGR}$, we applied the tight global relationship

between extreme drought-affected area and STD_{CGR} (Fig. 2c) and a spatial weight based on average FLUXCOM NEE to partition the changes in STD_{CGR} into the regional STD_{NEE} of each continent (i.e., tropical America, Africa, and Asia) and biome (i.e., tropical semi-arid and tropical forests), assuming the temporal relationship holds in the spatial dimension (see Methods). Over the three independent 20-year periods, the extreme droughts in tropical semi-arid ecosystem contributed more to STD_{NEE} than droughts in tropical forests. Among the three continents, droughts in tropical America incurred larger STD_{NEE} than those in tropical Africa and Asia (Fig. 3b, d, f), however, the dynamics of overall STD_{NEE} change were controlled by tropical Africa and Asia. The increase of STD_{NEE} from 1960 to 1979 to 1980 to 1999 was about 0.27 Pg C yr^{-1}, and tropical Asia and Africa contributed 0.14 Pg C yr^{-1} and 0.10 Pg C yr^{-1}, respectively. From 1980-1999 to 1997–2016, the decrease of STD_{NEE} was about 0.06 Pg C yr^{-1}, which was a net balance of decreasing extreme droughts and STD_{NEE} in tropical Africa and Asia—a total deduction of 0.17 Pg C yr^{-1} and increasing extreme droughts and STD_{NEE} in tropical America—a total increase of 0.11 Pg C yr^{-1} in STD_{NEE}. In comparison, DGVMs showed limited influence of extreme droughts on STD_{NEE} compared to STD_{CGR} but FLUXCOM detected a decrease in STD_{NEE} from 1980 to 1999 to 1997 to 2016.

Discussion

In this study, we find there were long-term changes in CGR variability (i.e., STD_{CGR}), which increased then decreased in the past six decades. The changes in STD_{CGR} were positively associated with changes in tropical extreme droughts and underlay previously unexplained dynamics of γ_{CGR}^{T} [8,10]. We find that extreme drought-affected area, which accounted for only 6–9% of the tropical vegetated surface, explained 75% of the variance in STD_{CGR}. The historical increase and the recent decrease in STD_{CGR} were dominated by drought area changes in tropical Africa and Asia, while tropical America showed monotonically increased drought area. In terms of biome contribution, tropical semi-arid ecosystems and forests contributed equally to the increase of STD_{CGR} in the 1980s and the 1990s but semi-arid ecosystems dominated the decrease in STD_{CGR} in the recent two decades. This study highlights the outsized role of tropical extreme droughts in influencing the long-term dynamics of CGR and amplifying γ_{CGR}^{T}, and has manifold implications for our current understanding of climate-carbon interactions.

Extreme events are known to influence the terrestrial carbon cycle[39], and drought is the most critical one[40]. Several studies have suggested that a few extreme events explained a significant amount of the variance in land-atmosphere carbon exchange, at seasonal or interannual time scales[41,42]. Here, our results show that extreme droughts influence CGR at the bi-decadal scale by amplifying STD_{CGR} and γ_{CGR}^{T}. Extreme droughts induce various concurrent and lagged effects on ecosystems[43], which include processes of either carbon emissions or carbon uptake. Though we find a tight correlation between extreme drought-affected area and STD_{CGR} (Fig. 2c), we acknowledge that the affected area is an integrated indicator of drought effects, which does not distinguish the various induced processes and their respective functioning time scales. Among the drought-induced effects, fire is unlikely to be the sole reason for the changes in STD_{CGR} as our analysis does not show a change in the long-term variability in fire emissions (Supplementary Fig. 2), meaning the role of other process needs further investigations. We suggest that extreme droughts in semi-arid ecosystems and tropical Africa and Asia deserve more attention for understanding long-term dynamics of the terrestrial carbon cycle.

In this study, we use nine competing linear models to derive γ_{CGR}^{T} and γ_{CGR}^{W} (Supplementary Fig. 1). The values of γ_{CGR}^{T} and γ_{CGR}^{W} and their long-term dynamics are highly influenced by the types of linear models and climate data used. Statistically, our result shows that γ_{CGR}^{W} is insignificant as long as the models include tropical temperature as a predictor. However, when using univariate linear models we note γ_{CGR}^{W} is significant (Supplementary Fig. 1h), caused by the strong correlation between ΔMAT and ΔTWS[15] or tropical lagged precipitation[44]. Previous studies have reported nonlinear responses of the tropical terrestrial carbon fluxes to temperature[45], VPD[46], precipitation[47], and soil moisture[23], which question the common practices of using linear models to derive γ_{CGR}^{T} and γ_{CGR}^{W} [6,8,9], though nonlinear models may not be statistically stronger than linear models with less degrees of freedom for fitting. To avoid the uncertainties in climate sensitivities incurred by the type of models and data used, we use STD_{CGR}, which is calculated from perhaps the least uncertain term in the global carbon cycle (i.e., CGR), as a proxy for γ_{CGR}^{T} to examine the long-term dynamics.

Tropical extreme droughts developed preferentially during El Niño events[48,49]. Therefore, the drought-STD_{CGR} correlation can also be interpreted as an El Niño Southern Oscillation (ENSO)-STD_{CGR} correlation. We use the Multivariate ENSO Index (MEI) to represent the frequency and strength of El Niño, and find MEI is positively related with ΔCGR, STD_{CGR} and the extreme drought-affected area ($p < 0.01$; Supplementary Fig. 4). The test shows ENSO not only modulates CGR at the interannual time scale[7], but also enhances the magnitude of CGR variability in periods with more frequent and stronger El Niño event by increasing extreme drought frequency. It is worth noting that MEI ($r^2 = 0.68$, Supplementary Fig. 4b) does not explain as much long-term variability in CGR as the extreme drought area ($r^2 = 0.75$, Fig. 2c).

DGVMs are unable to reproduce the tight positive relationship between STD_{CGR} and tropical extreme drought-affected area (Fig. 2d; Supplementary Fig. 5), indicating questionable representation of extreme drought in models. Most DGVMs show a negative correlation between extreme drought-affected area and STD_{NEE} (Fig. 2d, Supplementary Fig. 5b), which means extreme droughts cause limited land-atmosphere CO_2 exchange. This explains previously reported spatial asynchrony between carbon extremes and climate extremes in DGVMs[50], as carbon extremes in DGVMs are more likely driven by favorable climate than unfavorable climate extremes[51]. Missing components of drought–vegetation feedbacks (e.g., lagged effects) are potentially responsible for the biased estimates of NEE in DGVMs under extreme droughts. Previous studies have shown that in DGVMs droughts induce the largest impact during the climate extreme with little lagged influence[52], which is substantially shorter than observed drought effects lasting for several years[25,53]. With a focus only on transient stomatal control and soil moisture downregulattion[23], models generally lack enough mechanistic consideration of drought-induced legacy effects[27]. Moreover, ecosystems acclimate to temperature[54], CO_2[55], and extended droughts[56] to cope with water stress and adjust carbon uptake. Considering the increase in CO_2, temperature and drought frequency under future scenarios[38], these long-term trends indicate further biases in modeled STD_{NEE}.

FLUXCOM – a data-driven machine learning NEE product—was also unable to fully capture the dynamics in γ_{CGR}^{T} and STD_{CGR} (Fig. 1a, b). The underrepresentation of extreme droughts in the relatively short eddy covariance measurements (i.e., limited sites have more than 10 years of records)[57] and the lack of sites in the tropics[58] could lead to structural and long-term changes being undetected, and consequently to the underestimation of tropical NEE variability and CGR climate sensitivities. Other than the impact of extreme droughts, we acknowledge that the muted interannual variability of

FLUXCOM product may be also caused by the incapability of machine learning algorithms to capture low-frequency variations at the interannual time scale and the use of average remote sensing forcing[58]. However, unlike DGVMs, FLUXCOM identified a weak yet positive relationship between extreme drought-affected area and STD_{NEE} (Fig. 2d), showing that it has a better representation of extreme drought effects than DGVMs. It is worth noting that NEE of tropical extreme drought-affected regions from FLUXCOM shows a sensitivity of STD_{NEE} to the drought that is close to the sensitivity of STD_{CGR} to drought (Supplementary Fig. 5). To further improve the prediction of machine learning algorithms of CGR variability, one potential path is to use algorithms such as Long Short-Term Memory (LSTM) to incorporate the lagged effects of climate extremes into the simulation of terrestrial carbon fluxes[59].

Water is elemental to the function of terrestrial ecosystems, and is known to influence the terrestrial carbon cycle through processes at multiple temporal and spatial scales. Our analysis shows that extreme drought-affected area in the tropics is positively associated with the changes in STD_{CGR}, which explains the pronounced variations in γ_{CGR}^{T}, as CGR is more variable in decades when there are more extreme droughts. Our findings provide a quantitative basis to examine the drought-STD_{CGR} relationship, and provide a new perspective to understand carbon-water interactions over long periods.

Methods

Atmospheric CO_2 growth rate (CGR). We used CGR retrieved from the global average atmospheric CO_2 concentration reported by the US National Oceanic and Atmospheric Administration Earth System Research Laboratory (NOAA/ESRL)[60] and collated by the Global Carbon Project[61], for the period between 1959 and 2016. NOAA/ESRL has measured CO_2 for several decades at a globally distributed network of air sampling sites, including 4 baseline observatories (i.e., Barrow, Mauna Loa, Samoa and South Pole) and 8 tall towers, air samples collected by volunteers at more than 50 sites, and air samples collected regularly from small aircraft mostly in North America (https://www.esrl.noaa.gov/gmd/ccgg/about.html). For the period before 1980, the annual global CO_2 concentration is constructed on the measurements of two long-term baseline sites (Mauna Loa and South Pole) reported by Scripps Institute of Oceanography[62]. After 1980, the annual global CO_2 concentration is constructed by averaging half-hourly latitudinal CO_2 concentrations interpolated from the measurements of all NOAA/ESRL sites where samples are predominantly of well-mixed marine boundary layer[60]. CGR was then calculated by multiplying a factor of 2.124 GtC ppm^{-1} to the changes in atmospheric CO_2 concentration (ppm yr^{-1})[63].

Gridded Climate data. Global monthly gridded air temperature, precipitation and solar radiation data at 0.5° were provided by the Climate Research Unit (CRU) at University of East Anglia[64]. We used the CRU TS 4.01 climate dataset which ranges from 1959 to 2016. Monthly vapor pressure deficit was calculated as the difference between saturated vapor pressure calculated based on monthly air temperature and actual vapor pressure provided by CRU. Monthly soil water content at 0.5° was calculated from CRU climate data using the simple process-led algorithms for simulating habitats (SPLASH)[65]. SPLASH models soil water content as the residual of precipitation, runoff and evapotranspiration, with evapotranspiration calculated using a Priestly-Taylor scheme[66]. From the resulting monthly gridded climate dataset, we calculated mean annual tropical temperature (MAT), precipitation (MAP), solar radiation (RAD) and soil water content (SWC) for vegetated land. The correlation between the temporal dynamics of MAT and MAP is −0.15 (Pearson's r, $p = 0.27$), between MAT and SWC, −0.23 ($p = 0.09$), between MAP and SWC, 0.68 ($p < 0.01$). In addition, we used several other gridded climate datasets produced based on global observations available from 1959 to 2016 to examine the robustness of our results. These gridded climate datasets are Berkeley Earth Surface Temperature (BEST)[67], CRUTEM4 surface temperature[68], NASA Goddard Institute for Space Studies surface temperature (GISS)[69], global temperature and precipitation produced by University of Delaware (UDEL)[70], global precipitation produced by the Global Precipitation Climatology Centre (GPCC)[71] and NOAA's PRECipitation REConstruction over Land (PRECL)[72].

Ancillary remote sensing and modeled datasets. We used a reconstructed terrestrial water storage (TWS) derived from the GRACE satellite as one of observational proxies for tropical water availability. The reconstructed TWS ranges from 1981 to 2017 and has a global coverage at 0.5°[9]. We extracted TWS data over tropical vegetated land surface for our analysis. We used the Moderate Resolution Imaging Spectroradiometer (MODIS) MOD12 land cover product[73] to delineate

biome types in the tropics—forests (i.e., evergreen broadleaf forests) and semi-arid ecosystems (i.e., grasslands, shrublands and savanna type ecosystems). We used the land cover type that was most prevalent during the period 2000–2013 for our study area. Global fire carbon emissions were acquired from Global Fire Emission Database (GFED4s)[36]. Two estimates of global carbon emissions due to land use and land cover (LULC) were included in our analysis. One is an estimate based on two bookkeeping models used in the Global Carbon Project[61], the other one is an estimate based on a process-based model that considers the influences of climate variation and dynamic biomass density in the LULC emission[5].

Estimates of net ecosystem exchange (NEE). We used annual NEE estimated from two sources, including (1) 15 dynamic global vegetation models (DGVMs) from TRENDY v6[35] participating in the Global Carbon Project[61] and (2) FLUXCOM fluxes upscaled from eddy-covariance measurements using three machine learning methods[21].

DGVMs used in this study include CABLE, CLASS-CTEM, CLM4.5(BGC), DLEM, ISAM, JSBACH, JULES, LPJ-GUESS, LPJ, LPX-Bern, OCN, ORCHIDEE, ORCHIDEE-MICT, SDGVM, VISIT (Supplementary Table 1). These models were driven either by monthly CRU or 6-hourly CRU-NCEP gridded climate dataset and dynamic atmospheric CO_2 concentrations. Some models consider the effects of CO_2 fertilization, LULC, and nitrogen deposition on the carbon cycle, but carbon emissions due to LULC were considered separately thus not included in the NEE output. We used the DGVMs annual NEE estimates from 1959 to 2016.

FLUXCOM[21] estimates global NEE by upscaling measurements from 224 eddy-covariance flux tower sites using three different machine learning algorithms: Random forests (RF), Artificial Neural Networks (ANN) and Multivariate Adaptive Regression Splines (MARS). Each machine learning algorithm was trained on daily fluxes using 11 inputs including site-level meteorological data and mean seasonal cycle of MODIS observations. After obtaining the trained algorithm, gridded climatic variables from CRU-NCEP and the mean seasonal cycle of MODIS data were used to produce carbon flux estimates on 0.5°×0.5° grids and at monthly intervals. We then summed up the monthly gridded data and got the FLUXCOM annual NEE estimates from 1980 to 2013.

Climate sensitivity of CGR. We calculated the temperature sensitivity (γ_{CGR}^{T}) and the water sensitivity of CGR (γ_{CGR}^{W}) based on univariate or multivariate linear regressions of the anomalies of CGR (ΔCGR) on the anomalies of climate variables over tropical land. We defined anomalies as the departure to the fitted trend line of a time series[8,20]. We used nine competing models (M1 to M9) to derive γ_{CGR}^{T} and γ_{CGR}^{W} for every 20-year moving window, alternatively using the anomalies of tropical mean annual temperature (ΔMAT), mean annual precipitation (ΔMAP), mean shortwave radiation(ΔRAD), 4-month lagged precipitation (ΔMAP_{lag}), satellite-based terrestrial water storage (ΔTWS) and the interactions of temperature and water proxies as the predictors (Table 1; Supplementary Fig. 1). The interaction term was added in some models to account for the interaction of water and temperature variability, as suggested in a recent study[15]. We evaluated the performance of models based on their time range covered, adjusted coefficient of determination (Adj. R^2), Akaike information criterion (AIC) and variance inflation factor (VIF). In particular, large VIF indicates collinearity in predictors, which can generate instability in the coefficients of linear models, leading to more uncertain climate sensitivities. Long-term dynamics of γ_{CGR}^{T} and γ_{CGR}^{W} were qualitatively similar between the different multivariate models tested (Supplementary Fig. 1). We selected M1 (precipitation based) and M3 (TWS based) for the analyses presented in the main text, as they were less influenced by predictor collinearity -- evidenced by their lower VIF scores. CGR in the years 1991–1993 were affected by the eruption of Mt. Pinatubo and thus excluded from the analysis.

Quantifying drought-affected area. We used the percentiles of local monthly precipitation to detect droughts and drought-affected area. Though multiple aridity index can be used to do so, we chose monthly precipitation because (1) the indicator is directly related to IPCC definition of drought-"prolonged absence or marked deficiency of precipitation"[38] (2) some known uncertainties in the estimation of water demand – potential evapotranspiration – in the derivation of aridity indexes[74,75]. Droughts occur when monthly precipitation is below a certain local threshold in a reference period[76]. Specifically, for each pixel in the tropics, we converted its monthly precipitation from 1959 to 2016 to a percentile distribution. We defined the months that belong to the bottom 1% percentile of the precipitation as experiencing very extreme drought. By changing the choice of precipitation threshold (e.g., 1, 5, 10, 15, 20, 25, 30, 40, and 50%), we identified droughts of different severity for the pixel—the bottom 1% precipitation is very extreme drought, 1–10% is extreme drought, 10–25% is mild drought, and 25–50% is natural water deficits. To get the long-term dynamics of drought-affected area, for each 20-year span, we obtained the frequency of extreme drought (i.e., the ratio of the number of months experiencing droughts to the total number of months in the 20-year span) at the pixel level. The frequency was then used to weigh the area of pixels as we aggregated the drought-affected area to regional scales (e.g., tropic forests, semi-arid, continents, pantropic).

Quantifying the regional contributions to STD_{CGR}. Based on the tight correlation between extreme drought-affected area and STD_{CGR}, we adopted a time-for-space substitution to quantify regional (i.e., tropical America, tropical Africa, tropical Asia, tropical semi-arid ecosystems and tropical forests) contributions to STD_{CGR}, using the drought-affected area detected for these regions. To consider the spatial variation of regions in their land-atmospheric CO_2 exchange capacity, we used the multiyear average FLUXCOM NEE map as the spatial weight, as FLUXCOM NEE represents our best estimate of the spatial variation in NEE[58] and the product shows potential in capturing the extreme drought influence on NEE (Fig. 2d; Supplementary Fig. 5).

We note that to estimate the regional contribution of extreme droughts to STD_{CGR}, it is necessary to account for all transient and long-term carbon fluxes incurred by extreme droughts. In theory, this can be simulated in process-based DGVMs. But current DGVMs, as our results have suggested (Fig. 2d), inadequately capture the drought impacts on STD_{CGR}. Another option is to use remotely sensed aboveground biomass (AGB)[77] rather than data-driven NEE as the spatial weight. However, the method would imply that extreme droughts induced carbon losses proportionally to AGB. The assumption was questionable as drylands have less biomass but usually comparable net carbon exchange than wet forests[13,14]. Therefore, using the data-driven net flux product (i.e., FLUXCOM NEE) as a weight would be the preferred available option to approximate the regional contribution to STD_{CGR}, as FLUXCOM NEE showed potential in capturing the extreme drought influence on NEE (Fig. 2d; Supplementary Fig. 5). Importantly, our study is designed to provide a first-order quantification of the regional contribution to STD_{CGR} at coarse continental and biome scales, while the fine-scale variations at the pixel-level within each continent and biome remain to be addressed.

Remove the influence of autocorrelation. Autocorrelation is the correlation of a time series with a delayed copy of itself. Since we used a moving window to calculate STD_{CGR}, the value of STD_{CGR} in a window is not independent from its counterparts in adjacent windows, leading to autocorrelation in the time series of STD_{CGR}. In addition, since we calculated long-term variability in tropical water availability (e.g., $\overline{MAP}$, $\overline{SWC}$) using the same moving window, it can also generate some autocorrelation in these time series. To remove the influence of autocorrelation:

1) First, we introduced the Durbin-Watson indicator (DW) to evaluate the autocorrelation of these times series. We estimated the lag 1 autocorrelation in the residuals (e_i) from the ordinary linear regression of the variables of interest (e.g., STD_{CGR}, $\overline{MAP}$) to time, where the coefficient in the regression is ρ, as in $e_i = \rho e_{i-1} + r_i$. The DW tests the null hypothesis that residuals are uncorrelated (ρ = 0), against the alternative hypothesis that autocorrelation exists (ρ ≠ 0) (Eq. 1).

$$DW = \frac{\sum_{i=2}^{n}(e_i - e_{i-1})^2}{\sum_{i=1}^{n} e_i^2} \quad (1)$$

Where n is the number of observations, e_i is the ith residual of the linear regression of a target variable to time. The Durbin-Watson indicator (DW) is a value ranging between 0 and 4, where 0 means positive autocorrelation, 2 means no autocorrelation and 4 means negative autocorrelation.

2) We applied the Cochrane-Ocrutt procedure to adjust the variables of interests (y_i; e.g., STD_{CGR}, $\overline{MAP}$, $\overline{SWC}$, $\overline{TWS}$, $\overline{MAT}$, $\overline{VPD}$) to STD_{CGR_adj}, $\overline{MAP_{adj}}$, $\overline{SWC_{adj}}$, $\overline{TWS_{adj}}$, $\overline{MAT_{adj}}$ and $\overline{VPD_{adj}}$ where $y_{i\_adj} = y_i - \rho y_{i-1}$. After the procedure, we found the autocorrelations in STD_{CGR_adj}, $\overline{MAP_{adj}}$, $\overline{SWC_{adj}}$, $\overline{TWS_{adj}}$ and $\overline{MAT_{adj}}$ and $\overline{VPD_{adj}}$ were largely removed since their DW values were close to 2 − 1.6, 1.3 ± 0.1, 1.2, 1.3, 1.9 and 1.9 ± 0.03, respectively. Among them, $\overline{MAP_{adj}}$ and $\overline{TWS_{adj}}$ were negatively correlated to STD_{CGR_adj} with significance level of $p < 0.01$ and $p = 0.08$ (Fig. 2a), respectively, meaning the negative impact of long-term water availability on STD_{CGR} we found is significant after considering autocorrelation.

Furthermore, we conducted an alternative test to remove autocorrelation, in which we divided the 58-year CGR records into twelve independent 5-year segments (only the last segment has 2-year overlap with its previous segment), and calculated γ_{CGR}^{T}, γ_{CGR}^{W}, STD_{CGR} and the drought-affected area for each 5-year segment. Each 5-year segment is therefore independent from others since there is no overlap between them. Based on the γ_{CGR}^{T}, γ_{CGR}^{W}, STD_{CGR} and the drought-affected area from these 5-year segments, we re-examined their relationships to support our conclusion (Supplementary Fig. 3c, d).

Data availability

All data used in this study is publicly available. The Global Carbon Project dataset is archived at the website (https://www.icos-cp.eu/science-and-impact/global-carbon-budget/2017). The simulations from TRENDY DGVMs are available at https://sites.exeter.ac.uk/trendy. CRU TS4.01 can be accessed at https://crudata.uea.ac.uk/cru/data/hrg and CRU-NCEP can be accessed at https://crudata.uea.ac.uk/cru/data/ncep/. FLUXCOM dataset was downloaded from www.bgc-jena.mpg.de/geodb/projects/Data.php. Global Fire Emissions Database is accessible at http://www.globalfiredata.org/.

Berkeley Earth Surface Temperature can be downloaded from http://berkeleyearth.org/data/. Other auxiliary temperature and precipitation datasets are freely available at https://www.esrl.noaa.gov/psd/data/. We provide a processed dataset to support the reproduction and verification of the results at https://zenodo.org/record/5908612.

Code availability

All code that supports the finding of this study is available at https://zenodo.org/record/5908612.

References

1. Cox, P. M. et al. Sensitivity of tropical carbon to climate change constrained by carbon dioxide variability. *Nature* **494**, 341–344 (2013).
2. Bousquet, P. et al. Regional changes of CO_2 fluxes of land and oceans since 1980. *Science* **290**, 1253–1262 (2000).
3. Lee, K., Wanninkhof, R., Takahashi, T., Doney, S. C. & Feely, R. A. Low interannual variability in recent oceanic uptake of atmospheric carbon dioxide. *Nature* **396**, 155 (1998).
4. Le Quéré, C. et al. Trends in the sources and sinks of carbon dioxide. *Nat. Geosci.* **2**, 831 (2009).
5. Yue, C., Ciais, P., Houghton, R. A. & Nassikas, A. A. Contribution of land use to the interannual variability of the land carbon cycle. *Nat. Commun.* **11**, 3170 (2020).
6. Wang, W. et al. Variations in atmospheric CO_2 growth rates coupled with tropical temperature. *Proc. Natl Acad. Sci.* **110**, 13061–13066 (2013).
7. Keeling, C. D., Whorf, T. P., Wahlen, M. & van der Plichtt, J. Interannual extremes in the rate of rise of atmospheric carbon dioxide since 1980. *Nature* **375**, 666–670 (1995).
8. Wang, X. et al. A two-fold increase of carbon cycle sensitivity to tropical temperature variations. *Nature* **506**, 212–215 (2014).
9. Humphrey, V. et al. Sensitivity of atmospheric CO_2 growth rate to observed changes in terrestrial water storage. *Nature* **560**, 628–631 (2018).
10. Rödenbeck, C., Zaehle, S., Keeling, R. & Heimann, M. History of El Niño impacts on the global carbon cycle 1957–2017: A quantification from atmospheric CO_2 data. *Philos. Trans. R. Soc. B Biol. Sci.* **373**, 20170303 (2018).
11. Peylin, P. et al. Global atmospheric carbon budget: Results from an ensemble of atmospheric CO_2 inversions. *Biogeosciences* **10**, 6699–6720 (2013).
12. Fan, L. et al. Satellite-observed pantropical carbon dynamics. *Nat. Plants.* **5**, 944–951 (2019).
13. Poulter, B. et al. Contribution of semi-arid ecosystems to interannual variability of the global carbon cycle. *Nature* **509**, 600–603 (2014).
14. Ahlström, A. et al. The dominant role of semi-arid ecosystems in the trend and variability of the land CO_2 sink. *Science* **348**, 895 LP–895899 (2015).
15. Piao, S. et al. Interannual variation of terrestrial carbon cycle: Issues and perspectives. *Glob. Chang. Biol.* **26**, 300–318 (2020).
16. Wang, J., Zeng, N. & Wang, M. Interannual variability of the atmospheric CO_2 growth rate: Roles of precipitation and temperature. *Biogeosciences* **13**, 2339–2352 (2016).
17. Clark, D. A., Piper, S. C., Keeling, C. D. & Clark, D. B. Tropical rain forest tree growth and atmospheric carbon dynamics linked to interannual temperature variation during 1984-2000. *Proc. Natl Acad. Sci.* **100**, 5852–5857 (2003).
18. Doughty, C. E. & Goulden, M. L. Are tropical forests near a high temperature threshold? *J. Geophys. Res. Biogeosciences* **114**, 1–12 (2009).
19. Ballantyne, A. et al. Accelerating net terrestrial carbon uptake during the warming hiatus due to reduced respiration. *Nat. Clim. Chang.* **7**, 148–152 (2017).
20. Anderegg, W. R. L. et al. Tropical nighttime warming as a dominant driver of variability in the terrestrial carbon sink. *Proc. Natl Acad. Sci.* **112**, 201521479 (2015).
21. Jung, M. et al. Compensatory water effects link yearly global land CO_2 sink changes to temperature. *Nature* **541**, 516–520 (2017).
22. Humphrey, V. et al. Soil moisture – atmosphere feedback dominates land carbon uptake variability. *Nature* **592**, 65–69 (2021).
23. Green, J. K. et al. Large influence of soil moisture on long-term terrestrial carbon uptake. *Nature* **565**, 476–479 (2019).
24. Liu, Y., Kumar, M., Katul, G. G., Feng, X. & Konings, A. G. Plant hydraulics accentuates the effect of atmospheric moisture stress on transpiration. *Nat. Clim. Chang.* **10**, 691–695 (2020).
25. Phillips, O. L. et al. Drought–mortality relationships for tropical forests Oliver. *N. Phytol.* **187**, 631–646 (2010).

26. Bigler, C., Gavin, D. G., Gunning, C. & Veblen, T. T. Drought induces lagged tree mortality in a subalpine forest in the Rocky Mountains. *Oikos* **116**, 1983–1994 (2007).

27. Anderegg, W. R. L. et al. Pervasive drought legacies in forest ecosystems and their implications for carbon cycle models. *Science* **349**, 528–532 (2015).

28. Aragão, L. E. O. C. et al. Interactions between rainfall, deforestation and fires during recent years in the Brazilian Amazonia. *Philos. Trans. R. Soc. B Biol. Sci.* **363**, 1779–1785 (2008).

29. Schwalm, C. R. et al. Global patterns of drought recovery. *Nature* **548**, 202–205 (2017).

30. Huang, M., Wang, X., Keenan, T. F. & Piao, S. Drought timing influences the legacy of tree growth recovery. *Glob. Chang. Biol.* **24**, 3546–3559 (2018).

31. Chambers, J. Q., Higuchi, N., Schimel, J. P., Ferreira, L. V. & Melack, J. M. Decomposition and carbon cycling of dead trees in tropical forests of the central Amazon. *Oecologia* **122**, 380–388 (2000).

32. Berenguer, E. et al. Tracking the impacts of El Niño drought and fire in human-modified Amazonian forests. *Proc. Natl Acad. Sci.* **118**, e2019377118 (2021).

33. Ma, X. et al. Drought rapidly diminishes the large net CO_2 uptake in 2011 over semi-arid Australia. *Sci. Rep.* **6**, 1–9 (2016).

34. Sitch, S. et al. Evaluation of the terrestrial carbon cycle, future plant geography and climate-carbon cycle feedbacks using five Dynamic Global Vegetation Models (DGVMs). *Glob. Chang. Biol.* **14**, 2015–2039 (2008).

35. Sitch, S. et al. Recent trends and drivers of regional sources and sinks of carbon dioxide. *Biogeosciences* **12**, 653–679 (2015).

36. Van Der Werf, G. R. et al. Global fire emissions estimates during 1997-2016. *Earth Syst. Sci. Data* **9**, 697–720 (2017).

37. Ault, T. R. On the essentials of drought in a changing climate. *Science* **368**, 256–260 (2020).

38. IPCC. *Climate Change 2013: The Physical Science Basis. Contribution of Working Group I to the Fifth Assessment Report of the Intergovernmental Panel on Climate Change.* (Cambridge University Press, 2013). https://doi.org/10.1017/CBO9781107415324.

39. Reichstein, M. et al. Climate extremes and the carbon cycle. *Nature* **500**, 287 (2013).

40. Frank, D. et al. Effects of climate extremes on the terrestrial carbon cycle: Concepts, processes and potential future impacts. *Glob. Change Biol.* **21**, 2861–2880 (2015).

41. Zscheischler, J. et al. A few extreme events dominate global interannual variability in gross primary production. *Environ. Res. Lett.* **9**, 035001 (2014).

42. Von Buttlar, J. et al. Impacts of droughts and extreme-temperature events on gross primary production and ecosystem respiration: A systematic assessment across ecosystems and climate zones. *Biogeosciences* **15**, 1293–1318 (2018).

43. Anderegg, W. R. L., Berry, J. A. & Field, C. B. Linking definitions, mechanisms, and modeling of drought-induced tree death. *Trends Plant Sci.* **17**, 693–700 (2012).

44. Wang, J., Zeng, N. & Wang, M. Interannual variability of the atmospheric CO_2 growth rate: Roles of precipitation and temperature. *Biogeosciences* **13**, 2339–2352 (2016).

45. Tan, Z. H. et al. Optimum air temperature for tropical forest photosynthesis: Mechanisms involved and implications for climate warming. *Environ. Res. Lett.* **12**, 054022 (2017).

46. Green, J. K., Berry, J., Ciais, P., Zhang, Y. & Gentine, P. Amazon rainforest photosynthesis increases in response to atmospheric dryness. *Sci. Adv.* **6**, 1–10 (2020).

47. Guan, K. et al. Photosynthetic seasonality of global tropical forests constrained by hydroclimate. *Nat. Geosci.* **8**, 284–289 (2015).

48. Jiménez-Muñoz, J. C. et al. Record-breaking warming and extreme drought in the Amazon rainforest during the course of El Niño 2015-2016. *Sci. Rep.* **6**, 1–7 (2016).

49. Lyon, B. The strength of El Niño and the spatial extent of tropical drought. *Geophys. Res. Lett.* **31**, 1–4 (2004).

50. Ciais, P. et al. Europe-wide reduction in primary productivity caused by the heat and drought in 2003. *Nature* **437**, 529–533 (2005).

51. Zscheischler, J., Mahecha, M. D. & Buttlar, J. Von. A few extreme events dominate global interannual variability in gross primary production. *Environ. Res. Lett.* **9**, 035001 (2014).

52. Zscheischler, J. et al. Impact of large-scale climate extremes on biospheric carbon fluxes: An intercomparison based on MsTMIP data. *Glob. Biogeochem. Cycles* **28**, 585–600 (2014).

53. Saatchi, S. et al. Persistent effects of a severe drought on Amazonian forest canopy. *Proc. Natl Acad. Sci. U. S. A.* **110**, 565–570 (2013).

54. Williams, I. N., Torn, M. S., Riley, W. J. & Wehner, M. F. Impacts of climate extremes on gross primary production under global warming. *Environ. Res. Lett.* **9**, 094011 (2014).

55. Keenan, T. F., Luo, X., Zhang, Y. & Zhou, S. Ecosystem aridity and atmospheric CO_2. *Sci. (80-.).* **368**, 251.2–252 (2020).

56. Schuldt, B. et al. Change in hydraulic properties and leaf traits in a tall rainforest tree species subjected to long-term throughfall exclusion in the perhumid tropics. *Biogeosciences* **8**, 2179–2194 (2011).

57. Hawkins, L., Kumar, J., Luo, X., Sihi, D. & Zhou, S. Measuring, Monitoring, and Modeling Ecosystem Cycling. *Eos (Washington. DC).* **101**, (2020).

58. Jung, M. et al. Scaling carbon fluxes from eddy covariance sites to globe: Synthesis and evaluation of the FLUXCOM approach. *Biogeosciences* **17**, 1343–1365 (2020).

59. Besnard, S. et al. Memory effects of climate and vegetation affecting net ecosystem CO_2 fluxes in global forests. *PLoS One* **14**, 1–22 (2019).

60. Masarie, K. A. & Tans, P. P. Extension and integration of atmospheric carbon dioxide data into a globally consistent measurement record. *J. Geophys. Res.* **100**, 11593 (1995).

61. Le Quéré, C. et al. Global Carbon Budget 2018. *Earth Syst. Sci. Data* **10**, 2141–2194 (2018).

62. Keeling, C. D. et al. Atmospheric carbon dioxide variations at Mauna Loa Observatory, Hawaii. *Tellus* **28**, 538–551 (1976).

63. Ballantyne, A. P., Alden, C. B., Miller, J. B., Trans, P. P. & White, J. W. C. Increase in observed net carbon dioxide uptake by land and oceans during the past 50 years. *Nature* **488**, 70–73 (2012).

64. Harris, I., Jones, P. D., Osborn, T. J. & Lister, D. H. Updated high-resolution grids of monthly climatic observations - the CRU TS3.10 Dataset. *Int. J. Climatol.* **34**, 623–642 (2014).

65. Davis, T. W. et al. Simple process-led algorithms for simulating habitats (SPLASH v.1.0): Robust indices of radiation, evapotranspiration and plant-available moisture. *Geosci. Model Dev.* **10**, 689–708 (2017).

66. Priestley, C. H. B. & Taylor, R. J. On the Assessment of Surface Heat Flux and Evaporation Using Large-Scale Parameters. *Mon. Weather Rev.* **100**, 81–92 (1972).

67. Muller, A., Rohde, R., Jacobsen, R., R., Muller, E. & Wickham, C. A New Estimate of the Average Earth Surface Land Temperature Spanning 1753 to 2011. *Geoinformatics Geostatistics Overv.* **01**, 1–7 (2013).

68. Brohan, P., Kennedy, J. J., Harris, I., Tett, S. F. B. & Jones, P. D. Uncertainty estimates in regional and global observed temperature changes: A new data set from 1850. *J. Geophys. Res. Atmos.* **111**, 1–21 (2006).

69. Hansen, J., Ruedy, R., Sato, M. & Lo, K. Global surface temperature change. *Rev. Geophys.* **48**, 1–29 (2010).

70. Willmott, C. J. & Matsuura, K. Smart interpolation of annually averaged air temperature in the United States. *J. Appl. Meteorol.* **34**, 2577–2586 (1995).

71. Schneider, U. et al. Evaluating the hydrological cycle over land using the newly-corrected precipitation climatology from the Global Precipitation Climatology Centre (GPCC). *Atmosphere (Basel).* **8**, 30052 (2017).

72. Chen, M., Xie, P. & Janowiak, J. E. Global land precipitation: A 50-yr monthly analysis based on gauge observations. *J. Hydrometeorol.* **3**, 249–266 (2002).

73. Friedl, M. A. et al. MODIS Collection 5 global land cover: Algorithm refinements and characterization of new datasets. *Remote Sens. Environ.* **114**, 168–182 (2010).

74. Trenberth, K. E. et al. Global warming and changes in drought. *Nat. Clim. Chang.* **4**, 17–22 (2014).

75. Milly, P. C. D. & Dunne, K. A. Potential evapotranspiration and continental drying. *Nat. Clim. Chang.* **6**, 946–949 (2016).

76. Seneviratne, S. I. et al. Changes in climate extremes and their impacts on the natural physical environment. *Manag. Risks Extrem. Events Disasters Adv. Clim. Chang. Adapt. Spec. Rep. Intergov. Panel Clim. Chang.* **9781107025**, 109–230 (2012).

77. Baccini, A. et al. Tropical forests are a net carbon source based on aboveground measurements of gain and loss. *Science* **358**, 230–234 (2017).

Acknowledgements

Author contributions

X.L. and T.F.K. conceived the idea and designed the study. X.L. carried out the analysis. X.L. and T.F.K. wrote the paper.

Competing interests

The authors declare no competing interests.

Additional information

Supplementary information The online version contains supplementary material available at https://doi.org/10.1038/s41467-022-28824-5.

Correspondence and requests for materials should be addressed to Xiangzhong Luo or Trevor F. Keenan.

Peer review information *Nature Communications* thanks the anonymous reviewer(s) for their contribution to the peer review of this work. Peer reviewer reports are available.

Reprints and permission information is available at http://www.nature.com/reprints

Publisher's note Springer Nature remains neutral with regard to jurisdictional claims in published maps and institutional affiliations.